Adaptive OFDM Modulation for Underwater Acoustic Communications: Design Considerations and Experimental Results

Andreja Radosevic[†], *Student Member, IEEE,* Rameez Ahmed[‡], *Student Member, IEEE,* Tolga M. Duman[††], *Fellow, IEEE,* John G. Proakis[†], *Life Fellow, IEEE* and Milica Stojanovic[‡], *Fellow, IEEE*

[†]Dept. of Electrical and Computer Engineering, Univ. of California, San Diego
La Jolla, CA 92093, Email: aradosevic@ucsd.edu, proakis@ece.ucsd.edu

[††]School of Electrical, Computer and Energy Engineering, Arizona State University
Tempe, AZ 85287-5706, Email: duman@asu.edu

[‡]Dept. of Electrical and Computer Engineering, Northeastern University
Boston, MA 02115, Email: rarameez@gmail.com, millitsa@ece.neu.edu

Abstract

In this paper we explore design aspects of adaptive modulation based on orthogonal frequency division multiplexing (OFDM) for underwater acoustic (UWA) communications, and study its performance using real-time at-sea experiments. Our design criterion is to maximize the system throughput under a target average bit error rate (BER). We consider two different schemes based on the level of adaptivity:

This work is supported by the Multidisciplinary University Research Initiative (MURI) ONR Grants N00014-07-1-0738/0739, N00014-10-1-0576 and N00014-09-1-0700.

in the first scheme only the modulation levels are adjusted while the power is allocated uniformly across the sub-carriers, whereas in the second scheme, both the modulation levels and the power are adjusted adaptively. For both schemes we linearly predict the channel one travel time ahead so as to improve the performance in the presence of a long propagation delay. The system design assumes a feedback link from the receiver that is exploited in two forms: one that conveys the modulation alphabet and quantized power levels to be used for each sub-carrier, and the other that conveys a quantized estimate of the sparse channel impulse response. The second approach is shown to be advantageous, as it requires significantly fewer feedback bits for the same system throughput. The effectiveness of the proposed adaptive schemes is demonstrated using computer simulations, real channel measurements recorded in shallow water off the western coast of Kauai, Hawaii, in June 2008, and real-time at-sea experiments conducted at the same location in July 2011. We note that this is the first paper that presents adaptive modulation results for UWA links with real-time at-sea experiments.

Index Terms

Underwater acoustic communication, orthogonal frequency-division multiplexing (OFDM), adaptive modulation, feedback.

I. Introduction

Underwater acoustic (UWA) channels are considered as some of the most challenging communication media, generally characterized by low propagation speed of sound in water (nominally 1500 m/s), limited bandwidth and randomly time-varying multipath propagation which results in frequency-selective fading [1]. Delay spreading in an UWA channel can occur over tens of milliseconds; however, the channel impulse response often has a sparse structure, with only a few propagation paths carrying most of the channel energy.

Orthogonal frequency division multiplexing (OFDM) has recently emerged as a promising alternative to single-carrier systems for UWA communications because of its robustness to channels that exhibit long delay spreads and frequency selectivity [2]–[14]. However, applying OFDM to UWA channels is a challenging task because of its sensitivity to frequency offset

that arises due to motion. In particular, because of the low speed of sound and the fact that acoustic communication signals occupy a bandwidth that is not negligible with respect to the center frequency, motion-induced Doppler effects result in major problems such as non-uniform frequency shift across the signal bandwidth and inter-carrier interference (ICI) [15][16].

Time-varying multipath propagation and limited bandwidth place significant constraints on the achievable throughput of UWA communication systems. In order to support high spectral efficiencies over long time intervals in such non-stationary environment, we consider communication systems employing adaptive modulation schemes. While adaptive signaling techniques have been extensively studied for radio channels [17]–[21], only preliminary results for UWA channels are reported in [22] and [23], where simulations and recorded data are used to demonstrate the effectiveness of the proposed adaptation metrics.

The performance of an adaptive system depends on the transmitter's knowledge of the channel which is provided via feedback from the receiver. Since sound propagates at a very low speed, the design and implementation of an adaptive system essentially relies on the ability to predict the channel at least one travel time ahead. This is a very challenging task for communications in the range of several kilometers which imposes significant limitations on the use of feedback. However, our prior work has shown that channel prediction is possible over such intervals of time using a low-order predictor [24]. Crucial to successful channel prediction is motion compensation that stabilizes the non-uniform Doppler shift and enables (sparse) channel estimation. The so-obtained channel estimates contain only a few significant coefficients that are shown to be stable enough to support prediction several seconds into the future.

In this paper we design an adaptive OFDM system and study its performance using recorded test channels and real-time at-sea experiments. Our approach and contributions are the following:

- We estimate small Doppler rates (less then 10^{-4}) that correspond either to drifting of the instruments, or residuals after initial resampling in mobile systems (e.g. systems using autonomous underwater vehicles). Proper Doppler compensation ensures stability over in-

tervals of time that are long enough to support channel prediction several seconds ahead.

- We exploit the sparse multipath structure of the channel impulse response to estimate the most significant channel paths and simplify the prediction problem. Specifically, we estimate only a few significant paths of the channel within a possibly large overall delay spread. We treat the statistical properties of the underlying random process of the channel fading as unknown, and compute the parameters of a linear predictor adaptively, by applying a recursive least squares (RLS) algorithm [26].
- We develop two modulation schemes, distinguished by the level of adaptivity: Scheme 1 adjusts only the modulation level and assumes a uniform power allocation, while Scheme 2 adjusts both the modulation level and the power allotted to each sub-carrier. Both schemes are based on a greedy algorithm whose optimality was discussed in [20].
- We propose a new design criterion for an adaptive OFDM system based on the information that is fed back to the transmitter. Specifically, we consider two cases. In the first case, the information about the modulation alphabet and the quantized power level for each sub-carrier is computed at the receiver and fed back to the transmitter. In the second case, the quantized channel estimates are fed back, and the adaptive algorithm for bit-loading and power allocation is implemented at the transmitter.
- We demonstrate the effectiveness of the proposed adaptive schemes using computer simulations, test channels recorded during the Kauai Acoustic Communications MURI 2008 (KAM08) experiment in shallow water off the western coast of Kauai, Hawaii, in June 2008, and real-time at-sea experiments conducted during the Kauai Acoustic Communications MURI 2011 (KAM11) experiment at the same location in July 2011. The numerical and experimental results show that the adaptive modulation scheme can provide significant throughput improvements as compared to conventional, nonadaptive modulation for the same power and target BER.

The paper is organized as follows. In Section II, we describe the system and the channel model

that characterizes an UWA channel. In Section III, we introduce a linear RLS predictor for the channel tap coefficients. In Section IV, we introduce the rules for selection of the modulation levels, the information that is fed back to the transmitter, and the adaptive OFDM schemes. In Section V, we demonstrate the performance of the proposed adaptive schemes using numerical and experimental results that are based on recorded test channels and real-time at-sea trials, respectively. In Section VI, we provide concluding remarks.

II. System and Channel Model

Let us consider an OFDM system with K sub-carriers, where the n-th block of the input data symbols $X_{k,n}$, $k = 0, 1, \ldots, K-1$, is modulated using the inverse fast Fourier transform (IFFT). The block of input data consists of information-bearing symbols and pilots, with corresponding sets denoted as S_d and S_p, respectively. We assume that the information symbols are independent, while candidate modulation schemes are BPSK, QPSK, 8PSK and 16QAM with two-dimensional Gray mapping. In other words, for the k-th sub-carrier, where $k \in S_d$, and the n-th block, the modulation level $\mathcal{M}_{k,n} \in \{2, 4, 8, 16\}$, and if no data is transmitted $\mathcal{M}_{k,n} = 1$. It is assumed that the pilot symbols ($k \in S_p$) take values from the QPSK modulation alphabet. For each modulation alphabet, we assume a uniform distribution of the constellation points with a normalized average power. The transmitter sends frames of OFDM blocks, such that one OFDM block occupies an interval $T' = T + T_g$, where T and T_g are the symbol duration and the guard time interval, respectively. We denote by $B = K/T$ the total bandwidth of the system, by f_0 the frequency of the first sub-carrier, by $f_c = f_0 + B/2$ the central frequency, and by $\Delta f = 1/T$ the sub-carrier separation.

In this paper, we consider an adaptive system illustrated in Fig. 1. The different functional blocks of the system, such as channel and Doppler estimation, channel prediction, adaptive allocation, and feedback information, are discussed in the rest of the paper.

A. Channel Model

Let us now define the impulse response of the overall channel

$$h(\tau, t) = \sum_{p=0}^{P-1} h_p(t)\delta(\tau - \tau_p(t)), \tag{1}$$

where P is the number of distinct propagation paths, τ is the delay variable and t is the time at which the channel is observed. The coefficient $h_p(t)$ represents the real-valued gain of the p-th path, and $\tau_p(t)$ represents the corresponding delay. Here, we emphasize that the channel model (1) includes the initial resampling operation at the receiver by a common Doppler factor. Assuming a high bandwidth (sufficient resolution in the delay variable τ), the set of coefficients $\{h_0(t), \ldots, h_{P-1}(t)\}$ offers a good representation of the actual propagation paths. The received signal $r(t)$ is given as

$$r(t) = \sum_{p=0}^{P-1} h_p(t)s(t - \tau_p(t)) + n(t), \tag{2}$$

where $s(t)$ is the transmitted signal and $n(t)$ represents the additive white Gaussian noise (AWGN) process with zero-mean and power spectral density normalized to unity.[1] If we also define the equivalent baseband signals $u(t)$ and $v(t)$ with respect to the frequency f_c, such that

$$\begin{aligned} s(t) &= Re\left\{u(t)e^{j2\pi f_c t}\right\}, \\ r(t) &= Re\left\{v(t)e^{j2\pi f_c t}\right\}, \end{aligned} \tag{3}$$

we then obtain

$$v(t) = \sum_{p=0}^{P-1} c_p(t)u(t - \tau_p(t)) + w(t), \tag{4}$$

where

$$c_p(t) = h_p(t)e^{-j2\pi f_c \tau_p(t)}, \tag{5}$$

[1]The AWGN assumption incurs no loss of generality of the proposed adaptive scheme even though acoustic noise is not white.

and $w(t)$ is the equivalent baseband noise. Eq. (4) implies the equivalent baseband channel response

$$c(\tau, t) = \sum_{p=0}^{P-1} c_p(t)\delta(\tau - \tau_p(t)). \tag{6}$$

B. Modeling of the time-varying path delay $\tau_p(t)$

Following the approach from our previous work [24], we model the time-varying path delays as

$$\tau_p(t) = \tau_{p0} - \int_{x=0}^{t} a_p(x)dx, \tag{7}$$

where $a_p(t)$ is the Doppler scaling factor which is some function of time. This model includes the fixed term τ_{p0} which describes the nominal propagation delay corresponding to the system geometry at the time of transmission, and an additional term $\int_{x=0}^{t} a_p(x)dx$ that describes the effect of motion at the time of observation either due to drifting of the instruments (Doppler rates less then 10^{-4}) in stationary systems, or residuals after initial resampling in mobile systems (e.g. systems using autonomous underwater vehicles). The system motion during a period of time corresponding to a few seconds (or several data packets) is modeled by velocity and acceleration terms which lead to a linear Doppler rate $a_p(t)$. A more accurate model could include higher-order terms; however, experimental results confirm that this is not necessary. Specifically, we model $a_p(t)$ as a piecewise linear function

$$a_p(t) = a_p[n-1] + (a_p[n] - a_p[n-1])\left(\frac{t}{T'} - n + 1\right), \tag{8}$$

where $(n-1)T' \leq t \leq nT'$, and $a_p[n]$ are the Doppler scaling factors evaluated at time instances nT'.

This channel model is deemed suitable for the time scales of interest to an adaptive UWA communication system, since providing a reliable predicted channel state information (CSI) depends on the availability of a stable signal reference that can be obtained through accurate motion compensation. For example, for a 2 km link and the center frequency $f_c = 20$ kHz, a

small Doppler rate $a_p(t) \sim 10^{-5}$ can cause the phase of $c_p(t)$ in Eq. (5) to change up to π radians during a time interval of 1.33 seconds that corresponds to the propagation delay of one travel time.[2] Such a phase shift can considerably degrade the performance of channel prediction and the reliability of the corresponding CSI. In other words, proper Doppler compensation ensures stability over intervals of time that are long enough to support channel prediction several seconds ahead.

The model (7) allows one to decouple the phase $2\pi f_c \tau_p(t)$ into two terms, one that is not related to motion, and another that is related to motion. While the first term may not be predictable with sufficient accuracy because the frequency f_c may be several orders of magnitude larger than the inverse of the path delay, the second term can be predicted using the estimates of the Doppler scaling factors $a_p[n]$. With this fact in mind, we proceed to develop a channel prediction method that focuses on two general terms: a complex-valued coefficient $g_p(t) = h_p(t)e^{-j2\pi f_c \tau_{p0}}$, and a motion-induced phase $\theta_p(t) = 2\pi f_c \int_{x=0}^{t} a_p(x)dx$. In other words, we model the baseband channel response as

$$c(\tau, t) \;=\; \sum_{p=0}^{P-1} g_p(t) e^{j\theta_p(t)} \delta(\tau - \tau_p(t)) \tag{9}$$

where we treat each $g_p(t)$ as an unknown complex-valued channel coefficient, which is assumed to be stable over a prolonged period of time (tens of seconds), and $\theta_p(t)$ as an unknown motion-induced phase, which is modeled as a second-order polynomial based on the expressions (7) and (8). We emphasize that this model is valid for some interval of time, but its parameters may change from one such interval to another.

Our goal is to develop a two-step procedure in which we first estimate the channel coefficients at the receiver from a probe signal, and then use the so-obtained estimates to form predictions,

[2]Here we should make a distinction between making the prediction for one travel time ahead, and for the round-trip time (two travel times ahead), since the two cases correspond to different feedback implementation strategies, i.e. different functions performed by the two ends of a link.

which are finally fed back to the transmitter. This CSI will be used at the receiver (or the transmitter) to perform adaptive allocation of the modulation levels and power for each sub-carrier in the current OFDM block transmission.

C. Channel estimation

Channel estimation consists of two steps. In the first step, initial phase compensation is performed to produce a stable reference signal. This step includes resampling by a nominal (average) Doppler factor and removal of the phase offset $\theta_p(t)$. Here, we should emphasize that the process relies on the estimates of the Doppler scaling factors $a_p[n]$, which are assumed to be available with a certain precision (e.g. from a dedicated synchronization preamble). In the second step, the so-obtained signal is used to estimate the path coefficients $g_p(t)$. The Doppler factors are not needed thereafter, as we conjecture that the channel coefficients after motion-compensation exhibit sufficient stability to allow prediction several seconds into the future.

Fig. 2 illustrates the channel estimates obtained from real data collected during the KAM08 experiment. Specifically, in this subsection we will focus on channel estimates obtained from a short probe signal described in [25]. After the initial phase compensation where a phase-locked loop (PLL) was used, we perform channel estimation from the received signal using the matching pursuit (MP) algorithm [27]. Note from Fig. 2 that the MP algorithm produces 8 coefficients, where neighboring coefficients belong to the same propagation path due to the path dispersion [1]. For further analysis we weigh the adjacent coefficients based on the channel tap power and merge them, so as to represent the channel via four propagation paths g_0, g_1, g_2 and g_3. Therefore, the MP algorithm provides estimates of the channel coefficients $g_p(t)$, assuming that $P = 4$ channel coefficients are sufficient for the description of the sparse multipath structure. These estimates are denoted by $\tilde{g}_p[n]$, and computed at time instances nT' separated by $T' = 155$ ms. For comparison purposes, we also provide the channel estimate obtained using the RLS algorithm. Different peaks in the channel estimates can be associated with multiple surface and bottom

reflections calculated from the geometry of the experiment. As it can be seen from the figure, the MP algorithm successfully estimates the significant channel coefficients, and reduces the estimation error with respect to that incurred by the RLS algorithm.

We emphasize that positions of the significant paths may drift on a larger time scale (tens of seconds), and therefore have to be updated accordingly. In Fig. 3, we show the magnitudes and phases of the significant paths over a time period of 8 s. As we initially conjectured, the phases of $g_p(t)$ remain relatively stable for more than a few seconds (a propagation delay over several kilometers).

III. Channel Prediction

As we previously reported in [24], the future values of $g_p(t)$ are predicted from the estimates $\tilde{g}_p(t)$. In particular, if the OFDM blocks are periodically transmitted at time instances $t = nT'$, we use M observations made at times $n, n-1, ..., n-M+1$ to predict the channel at time $n+1$. To account for possible correlation between the path coefficients, we allow for their joint prediction. In other words, we use all P channel coefficients to predict each new coefficient. The prediction is thus made as

$$\hat{\mathbf{g}}[n+1] = \mathbf{W}^H[n]\tilde{\mathbf{g}}_M[n], \tag{10}$$

where

$$\hat{\mathbf{g}}[n+1] = [\tilde{g}_0[n+1]\ \tilde{g}_1[n+1]\ \ \ldots\ \ \tilde{g}_{P-1}[n+1]]^T, \tag{11}$$

$$\tilde{\mathbf{g}}_M[n]\ =\ [\tilde{g}_0[n]\ldots\tilde{g}_0[n-M+1]\tilde{g}_1[n]\ldots\tilde{g}_1[n-M+1]\tilde{g}_{P-1}[n]\ldots\tilde{g}_{P-1}[n-M+1]]^T. \tag{12}$$

The matrix $\mathbf{W}[n]$ contains $MP \times P$ prediction coefficients that are to be determined.

Because the second-order statistics are not available for the random process $\mathbf{g}[n+1]$, we compute $\mathbf{W}[n]$ adaptively, by applying the RLS algorithm as specified in Table I. In Eq. (21), $\mathbf{R}$ is an $MP \times MP$ matrix which represents an estimate of the inverse joint auto-correlation

matrix $E\left\{\tilde{\mathbf{g}}_M[n]\tilde{\mathbf{g}}_M^H[n]\right\}$ and δ is a small constant, typically a fraction of the minimum among variances of the channel coefficients jointly predicted by the RLS algorithm.

As discussed earlier, UWA systems suffer from inherently long propagation delays, which pose additional challenges in the design of a predictor. To counteract this problem, channel prediction one travel time ahead is achieved by using an RLS predictor of a low order M (e.g. $M = 1$ or $M = 2$) and a small forgetting factor λ (e.g. $\lambda = 0.5 \sim 0.75$, which corresponds to an effective window of length $L_{eff} = 1/(1-\lambda) = 2 \sim 4$). Note that the forgetting factor λ is uniquely specified for all P channel coefficients. With a small order M and only a few significant paths, i.e. a small P, computational complexity of joint channel prediction is sufficiently low to allow for a practical implementation.

The structure of the matrix $\mathbf{W}[n]$ is primarily driven by the geometry of the propagation environment, i.e. not all of the propagation paths are mutually correlated. In the present data set, the strongest arrival often exhibits more stability, and the contribution from the other, weaker paths in its prediction appears to be negligible. Therefore, the strongest path can be predicted independently, without loss in performance. In other words, if the channel coefficient k corresponds to the strongest path, Eq. (25) can be modified as follows: the k-th column of $\mathbf{W}[n]$ is recursively updated only for those elements that correspond to the prior observations of the k-th coefficient ($\tilde{g}_k[n], \tilde{g}_k[n-1], \ldots, \tilde{g}_k[n-M+1]$). In addition, exploiting the correlation among the remaining paths may lead to a performance improvement, whose exact amount is determined by the environmental profile, and accuracy of the channel and Doppler estimates.

After performing channel prediction at the receiver, the so-obtained CSI is used to initialize adaptive allocation of the modulation levels and power across the OFDM sub-carriers. As we will discuss later, depending on which end of the communication link performs adaptive allocation, different types of information are fed back over a low-rate feedback channel. In the following, we describe the design framework, initially proposed in [23], under which we developed two practical adaptive modulation schemes, and we also discuss the design of band-limited feedback.

IV. Adaptive Modulation and Power Allocation

The system model assumes that residual Doppler effects are negligible after proper initial motion compensation (resampling by a nominal Doppler factor and removal of the phase offset $\theta_p(t)$). After this initial step, it is also assumed that the channel is constant at least over the transmission interval T of one OFDM block. Therefore, the received signal can be expressed as

$$Y_{k,n} = G_{k,n}\sqrt{C_{k,n}}X_{k,n} + N_{k,n}, \tag{13}$$

where

$$G_{k,n} = \sum_{p=0}^{P-1} g_p[n]e^{-j2\pi(k\Delta f - B/2)\tau_{p0}}, \tag{14}$$

and $Y_{k,n}$, $C_{k,n}$, and $N_{k,n}$ are, respectively, the received signal after fast Fourier transform (FFT) demodulation, the transmitted power, and zero-mean circularly symmetric complex AWGN with variance $\sigma_N^2/2$ per dimension. The noise term includes the effects of ambient noise and residual ICI on the k-th sub-carrier and the n-th OFDM block, which is approximated as a Gaussian random variable.

For the transmission of each OFDM block we adaptively compute the size of the modulation alphabet $\mathcal{M}_{k,n}$ and the transmission power $C_{k,n}$. The objective of our adaptive OFDM system is to maximize the throughput by maintaining a target average BER. In order to maintain the BER at a fixed value, we propose the following optimization criterion:

$$\begin{aligned} \underset{\mathcal{M}_{0,n},\ldots,\mathcal{M}_{K-1,n}}{\text{maximize}} \quad & \sum_{k=0}^{K-1} \log_2 \mathcal{M}_{k,n} \\ \text{subject to} \quad & \sum_{k=0}^{K-1} C_{k,n} \leq C_n, \\ & \frac{1}{K}\sum_{k=0}^{K-1} P_{e,k} = P_b, \end{aligned} \tag{15}$$

where C_n is the overall average power allocated to the n-th OFDM block, $P_{e,k}$ is the average BER for the k-th sub-carrier, and P_b is the target average BER. The average power can be expressed as $C_n = C + C_{n-1}^{res}$ where C is a constant and C_{n-1}^{res} is the residual power from the

previous block which was not allocated (i.e., C_{n-1}^{res} is less than the minimum power increment required by the algorithm for a one-bit increase of the overall throughput). Here, we should emphasize the difference between total power allocation and distribution of this total power among the sub-carriers. In the former case, one can design an adaptive scheme where the total power C is adaptively allocated (and uniformly distributed among the sub-carriers) in order to achieve the prespecified performance (e.g. the target average BER or SNR at the receiver) for the *fixed* system throughput, whereas in the latter case, the fixed total power C is non-uniformly distributed among the sub-carriers to achieve the prespecified performance, and to *maximize* the system throughput. For the purpose of experimental sea-trials, the total power allocation C is initially set to a value which is able to support the target error rate, and avoid the outage scenario (no data transmission).

In order to reduce the computational complexity of the adaptive algorithm, the sub-carriers of the n-th OFDM block can be grouped into clusters. If we assume $K = 2^d$, we group consecutive sub-carriers into $Q = 2^{d_Q}$ clusters, where $K/Q = 2^{d-d_Q}$ is the size of each cluster. We denote by $C_{q,n}^Q$ and $\mathcal{M}_{q,n}^Q$, respectively, the allocated power and the modulation level corresponding to the q-th cluster, $q = 0, 1, \ldots, Q-1$. The optimal power level for each cluster q depends on the transfer function of the channel. If the channel does not change much within a cluster, computation of $C_{q,n}^Q$ and $\mathcal{M}_{q,n}^Q$ is performed based on the average channel gain in cluster q. Note that if a cluster is affected by a deep fade, it will be dominated by the sub-carrier with the lowest channel gain. Clustering reduces the computational load (see [23] for more details), but implies possible error penalization and/or a decrease in throughput as compared to the full computation of modulation levels and powers for all sub-carriers.

A. Thresholds for modulation levels $\mathcal{M}_{k,n}$

Due to the large propagation delays, the proposed adaptive OFDM transmission relies on channel prediction. We obtain predictions of the channel gains $G_{k,n}$ one travel time ahead based

on the time-domain predictions of the most significant channel coefficients (10). We model the prediction error on the p-th channel path as a complex zero-mean circularly symmetric Gaussian random variable with variance $\sigma_{e,p}^2/2$ per dimension. Furthermore, based on the *a priori* knowledge obtained from the channel prediction, we model $G_{k,n}$ as a complex Gaussian random variable with mean

$$\widehat{G}_{k,n} = \sum_{p=0}^{P-1} \hat{g}_p[n] e^{-j2\pi(k\Delta f - B/2)\tau_{p0}}, \tag{16}$$

and variance $\sigma_e^2 = \sum_{p=0}^{P-1} \sigma_{e,p}^2$, where P is the number of significant time-domain channel coefficients. Assuming that the current channel gain $G_{k,n}$ is perfectly known, we apply maximum likelihood symbol detection for the AWGN channel at the output of the matched filter. Thus, the probability of bit error for the k-th sub-carrier for MPSK/MQAM is well approximated by [18]

$$P_k(G_{k,n}, C_{k,n}, \mathcal{M}_{k,n}) \approx 0.2 e^{-\frac{m(\mathcal{M}_{k,n})}{2(\mathcal{M}_{k,n}-1)} \frac{C_{k,n}}{\sigma_N^2} |G_{k,n}|^2}, \tag{17}$$

where the coefficients $m(\mathcal{M}_{k,n})$ are determined numerically for each modulation alphabet, as accurately as desired for the BER approximation and take values $2.2, 3.3, 3.5$ and 3.6 for $\mathcal{M}_{k,n} = 2, 4, 8$ and 16, respectively.

For transmission of the n-th OFDM block, the adaptive system has knowledge of the predicted values $\widehat{G}_{k,n}$, but not of the full channel $G_{k,n}$. Therefore, from Eq. (17), the average BER on the k-th sub-carrier is obtained as [18]

$$\begin{aligned} P_{e,k} &\approx E\left[P_k(G_{k,n}, C_{k,n}, \mathcal{M}_{k,n}) | \widehat{G}_{k,n}\right] \\ &\approx 0.2 \frac{\exp\left(-\frac{|\widehat{G}_{k,n}|^2}{\sigma_e^2}\left(1 - \frac{1}{1+\frac{m(\mathcal{M}_{k,n})}{2(\mathcal{M}_{k,n}-1)}\frac{C_{k,n}}{\sigma_N^2}\sigma_e^2}\right)\right)}{1 + \frac{m(\mathcal{M}_{k,n})}{2(\mathcal{M}_{k,n}-1)}\frac{C_{k,n}}{\sigma_N^2}\sigma_e^2}. \end{aligned} \tag{18}$$

For a given target $P_{e,k}$, we now compute the thresholds $C_{k,n}^*(\mathcal{M}_{k,n})$ for the available modulation levels. The solution for $C_{k,n}^*(\mathcal{M}_{k,n})$ is given by

$$C_{k,n}^*(\mathcal{M}_{k,n}) = \frac{2(\mathcal{M}_{k,n}-1)\sigma_N^2}{m(\mathcal{M}_{k,n})\sigma_e^2} \left\{ \frac{|\widehat{G}_{k,n}|^2}{\sigma_e^2} \left[\mathcal{W}_0\left(\frac{|\widehat{G}_{k,n}|^2}{\sigma_e^2} e^{\left(\frac{|\widehat{G}_{k,n}|^2}{\sigma_e^2} + \ln\frac{P_{e,k}}{0.2}\right)} \right) \right]^{-1} - 1 \right\}, \tag{19}$$

where $\mathcal{W}_0(x)$ ($x > -1/e$) is the principal branch of the Lambert $\mathcal{W}$-function, the inverse function of $x = W\exp(W)$. Note that, if $|\widehat{G}_{k,n}|^2/\sigma_e^2 \gg \ln(P_{e,k}/0.2)$, the threshold goes to zero, i.e. $C^*_{k,n}(\mathcal{M}_{k,n}) \to 0$. This case corresponds either to high SNR regimes with reliable CSI, or to very high target BERs of the system. Reasonably accurate approximations for $\mathcal{W}_0(x)$, which can be computed efficiently, are provided in [28]. We should emphasize that different thresholds correspond to different average values of $\widehat{C}_{k,n}$, since all of the sub-carriers are affected by the prediction error of the same variance σ_e^2.

The optimization problem (15) is hard to solve from the standpoint of a practical implementation, because it is computationally too intensive to be run at the receiver (or the transmitter) for every OFDM block. Therefore, we pursue sub-optimal solutions which are obtained by relaxing one of the problem constraints. Specifically, we focus on two adaptive schemes in the rest of this section.

B. Adaptive Scheme 1

The optimal solution for (15) includes a non-uniform power allocation for a maximum attainable throughput, such that the target average BER is P_b. This causes that each sub-carrier contributes to the average BER differently, due to the frequency selectivity of the channel. However, the problem can be simplified if we consider adaptive allocation of the modulation levels while distributing the power uniformly among the sub-carriers. Since we adaptively allocate only the modulation levels, the so-obtained solution for (15) will be sub-optimal. Specifically, we apply a greedy algorithm that computes the modulation levels in a given block n using the allocations from the previous block $n-1$ for initialization. The proposed algorithm is given in Table II. Similar greedy algorithms have already been considered in [29] and [30].

After initialization of the algorithm for each sub-carrier, as given by Eqs. (27)–(30), we successively increase the modulation levels for those sub-carriers that require the smallest power increment (31)–(43), while maintaining the average BER below the target P_b. If the set of

modulation levels from the previous transmission interval is not a greedy-based solution for the currently available CSI $\{\widehat{G}_{k,n}\}$, the algorithm greedily searches for the closest solution which is used as a new initialization point of the algorithm. Also, if the algorithm does not support the throughput from the previous transmission interval (i.e., it fails during the initialization step), it searches for the sub-carrier k^* with the largest power decrement that is required in order to decrease the modulation level $\mathcal{M}_{k^*,n}$. The algorithm is terminated when the pre-specified P_b is achieved.

C. Adaptive Scheme 2

In the second scheme we consider adaptive allocation of the modulation levels and the sub-carrier powers such that $P_{e,k} = P_b$ for each sub-carrier.

Once the thresholds are computed from (19), we apply the adaptive algorithm of Table III to generate the signal of the n-th OFDM block. The algorithm is terminated when the available power C_n is exhausted, or when all sub-carriers achieve the maximum modulation level (16QAM). Here, we emphasize that for those sub-carriers that are in a deep fade no data is transmitted (zero power is allocated). In other words, the sub-carrier with index k is in deep fade if the threshold $C^*_{k,n}(\mathcal{M}_{k,n})$ is high enough to violate the power constraint in Eq.(15).

Because of the additional freedom to adjust the power, this scheme will achieve a higher overall throughput as compared to Scheme 1.

D. Limited feedback for adaptive UWA systems

We assume that a limited-feedback channel is available for conveying information from the receiver back to the transmitter. Two types of feedback information are considered in this paper: the modulation alphabet and the quantized power levels for each sub-carrier/cluster, or the quantized estimate of the sparse channel impulse response.

If the channel changes slowly across frequencies, neighboring sub-carriers are allocated the same modulation and power levels. In such a case, it is not necessary to feed back the channel

information for each sub-carrier, i.e., the total number of bits that are fed back can be reduced. Moreover, the power levels can be uniformly quantized, such that L_c bits are used to represent each quantization level. Also, L_m bits are used to represent the available modulation levels. For example, in our case we describe four modulation levels using $2^{L_m} = 8$ indices, which is more than the needed minimum. In contrast, $P(2L_g + L_t)$ bits are required to convey the information about P significant coefficients in the channel impulse response, assuming that $2L_g$ bits and L_t bits are required to represent the quantized complex gain and the delay of each dominant channel coefficient, respectively.

Due to the long propagation delay and time-division duplexing, we assume a feedback channel which imposes a limit on the maximum number of bits that can be conveyed to the transmitter. Therefore, lossless data compression techniques can be used at the receiver to reduce the number of bits that are conveyed back to the transmitter. For example, Run–Length–Encoding (RLE) [31] is a simple coding scheme that provides good compression of data that contains many runs of zeros or ones. It can be applied together with the well-known Lempel–Ziv–Welch (LZW) code [32] (used as an inner code), to efficiently compress the feedback information. As we will see in the following section, assuming perfect channel state information (CSI) at the receiver, feeding back the channel state information about the sparse multipath structure and making the decision on the transmitter side is shown to be advantageous since it requires significantly fewer bits.

V. Numerical and Experimental results

In this section we present numerical and experimental results on the performance of the proposed adaptive schemes from Sec. IV. The numerical results are based on channel measurements recorded during the KAM08 experiment, and experimental results from the real-time at-sea trials that were conducted during the KAM11 experiment. Both experiments were conducted at the same location with operational areas marked in Fig. 4.

A. Numerical results from the KAM08 experiment

The KAM08 experiment took place in 100 m deep water, with a communication distance of 4 km. The transmitter was deployed at the location Sta00 (see Fig. 5) as a 52.5 m aperture vertical array of 8 ITC-1001 transducers (7.5 m spacing), with a sampling rate of $f_{s,Tx} = 100$ kHz. The receiver was deployed at the location Sta08 as a 56.25 m aperture vertical line array (VLA) of 16 elements (3.75 m spacing), with a sampling rate of $f_{s,Rx} = 50$ kHz. The performance results are based on the channel estimates for transmissions between the fourth transducer from the bottom (49.5 m deep) and the tenth hydrophone from the bottom (65.25 m deep). The total bandwidth and the guard time are $B = 7.8$ kHz and $T_g = 150$ ms, respectively. We assume an OFDM transmission with $K = 512$ sub-carriers and a frequency separation of 15.25 Hz. The target average BER is $P_b = 10^{-3}$. We estimate the channel using the MP algorithm, and predict the five significant channel coefficients 2.67 s ahead.

Fig. 6 presents achievable throughput results for the OFDM systems that employ Scheme 1 and Scheme 2 without clustering for $\sigma_e^2 = -24$ dB, which is measured relative to the overall channel power. We also provide performance results for the non-adaptive scheme (with uniform power and modulation levels) and the optimal solution, which is evaluated using the interior-point method [33] to solve the nonlinear convex optimization problem (15). Interestingly, Scheme 2 shows a slight performance loss only for the high SNR regime as compared to the optimal solution, while Scheme 1 exhibits a performance degradation for the entire SNR region. Both schemes significantly outperform the non-adaptive solution.

In Fig. 7 we summarize the feedback requirements of Scheme 2 without clustering ($Q = 1$). Feeding back the power and modulation level computed at the receiver clearly requires more bits than feeding back the (sparse) channel response. $L_c = 2, 3, 4$ and 5 bits are used to represent the quantized power levels, and $L_m = 3$ bits are used to represent the five modulation levels (no transmission, BPSK, QPSK, 8PSK and 16QAM), resulting in a total of $2560, 3072, 3584$ and 4096 bits with $K = 512$ and $Q = 1$. The feedback information is then compressed as

discussed in Sec. IV, resulting in 201, 245, 294 and 350 bits (the values indicated on the x-axis). If the channel response is fed back, $L_g = 3, 4, \ldots, 10$ bits are used to represent the real and the imaginary parts of each quantized channel coefficient, and $L_t = 8$ bits are used to represent the corresponding delays. The feedback information is then compressed similarly as in the previous strategy. We note that the minimum number of bits required to maintain the target average BER at 10^{-3} is 350 and 120 for the two cases, i.e. that feeding back the channel response reduces the feedback requirements approximately three fold. When clustering is applied, the two feedback strategies require a similar number of bits to feed back; however, clustering is performed at the expense of reducing the overall throughput of Scheme 2.

B. Experimental results from the KAM11 experiment

The KAM11 experiment took place in $100-120$ m deep water, with communication distances of 1, 2 and 3 km. The transmitter was deployed from the ship as a 1.5 m aperture vertical array of 4 ITC-1032 transducers (0.5 m spacing) at different locations within the operational area while the ship was stationary. The sampling rate was $f_{s,Tx} = 100$ kHz. The RF-coupled receiver was deployed at the location Sta05 and Sta10 (see Fig. 8) as a 0.6 m aperture VLA of 4 elements (0.2 m spacing), with a sampling rate of $f_{s,Rx} = 100$ kHz. Both the transmitter and the receiver were deployed in the middle of the water column. A feedback from the recorder buoy was provided using an RF link. The geometry of the experiment and the setup of the system are given in Fig. 9. Due to the variations of the channel that are inherently present, and different communication distances tested in the field, a typical SNR at the receiver varied between 2 and 20 dB.

The OFDM frame contains 4 blocks with $K = 1024$ sub-carriers per block, at a central frequency of $f_c = 30$ kHz. The receiver operates coherently where 50% of sub-carriers are used as pilots to accommodate for real-time testing of the system, since the channel multipath structure can significantly change during an experimental trial (tens of minutes or even hours).

Note that such a high overhead will not be required in practice when a propagation model can be run prior to deployment to evaluate the multipath extent for a given system geometry. The total bandwidth and the guard time are $B = 10$ kHz and $T_g = 100$ ms, respectively. Frame synchronization is performed using a PN-sequence of duration 25 ms and the symbol rate 10 ksymb/s. The presented performance results are generated by employing maximal ratio combining (MRC) of signals received at four elements. However, we should emphasize that even though MRC is used for data detection, we use only one receive element to perform channel estimation and adaptive allocation in order to minimize the processing time at the receiver.

The adaptive system is initialized at the transmitter-end (a terminal at the ship) by sending activation commands to the receiver-end (a terminal at the RF-coupled buoy) through the wireless link. Once a confirmation message is received from the receiver terminal, the transmitter-end execute a sequence of operations such as acquiring the ship position from GPS, gathering various environmental data, etc. This is followed by the first OFDM frame transmission with a uniform power allocation and QPSK modulation alphabet for all data sub-carriers. Once the frame is detected at the receiver, it is stored at the local driver for further processing. In particular, we perform initial synchronization using the PN-preamble, which is followed by PLL-based Doppler estimation and compensation as suggested in [15]; we then conduct channel estimation over the uniformly-spaced pilot grid using the orthogonal matching pursuit (OMP) algorithm [27], and perform coherent detection for each OFDM block of the received frame; finally, using the channel estimates, we execute Scheme 2 at the receiver to compute the power and modulation levels, which are then fed back to the transmitter and used for the next OFDM frame transmission. During each real-time trial, we transmitted between 30 and 50 consecutive OFDM frames in order to demonstrate the performance of the proposed adaptive scheme, and the functionality of the implemented system.

Among various constraints on the real-time implementation of the system (e.g. out-of-band interference from the other systems simultaneously tested, a weak RF link for certain positions

of the ship, weather conditions, etc.), the most important limitation is determined to be the total round-trip time of the system that was on the order of $10-20$ s. This significant delay was mainly caused by all-level processing of the system at both sides of the link (acquiring GPS and environmental data before each transmission, and after each reception, data detection, recording, and data processing, including prediction and adaptive allocation, etc.), while physical propagation contributed with delays of $0.67-2$ s. Note that the RF feedback imposes no significant delay in the system. Since the total round-trip time is mainly limited by high processing delays, a good performance of the proposed schemes is expected for the channels with the coherence time of several seconds. In contrast, for rapidly-varying channels, high processing delays will result in a poor performance of channel prediction and outdated CSI. Here, we should emphasize that the ultimate performance limitation of an adaptive UWA system will not be determined by the processing delay, but by the physical propagation delay, which gives a lower bound on the channel coherence time that can be supported.

As discussed in Sections II and III, some channel measurements indicated that the channel coherence time was $3-4$ seconds (or more), which allowed us to perform channel prediction. Therefore, in the rest of this section, we will focus on the experimental results obtained from sea-trials during which channel conditions were calm (e.g. wind speed of $2-8$ knots and Doppler rates of 10^{-4}), and the (average) channel coherence time is on the order of seconds. We note that channel conditions in general may not be so calm, resulting in a proportional reduction of coherence times that can severely limit the performance of our adaptive scheme.

In Fig. 10 we show the channel estimates obtained from the frame synchronization preamble of a 2 km link for three consecutive non-adaptive QPSK-modulated OFDM frame transmissions, labeled as a, b and c. As mentioned earlier, the average time interval between two consecutive frame transmissions is (roughly) 20 s. Note the significant variations of the channel impulse response within a one-minute time interval. For the given consecutive OFDM frame transmissions, in Fig. 11 we provide the performance results for the receiver with four elements. Note

that poor performance is achieved for transmissions a and b, while a fair performance is obtained for transmission c, corresponding to very high SNR observed at the receiver (see Fig. 10). If the target average BER for OFDM systems is set to $10^{-2} - 10^{-3}$, the non-adaptive scheme should use either more power, or reduce the overall throughput by employing the BPSK modulation alphabet which is preferable for the power limited systems.

In Fig. 12 we illustrate channel estimates of a 2 km link for three consecutive adaptive OFDM frame transmissions, labeled as a, b and c. The available adaptive modulation alphabets are BPSK, QPSK and 8PSK. As in the previous set of non-adaptive OFDM block transmissions, we note significant variations in the channel impulse response within an one-minute time interval. For the given consecutive OFDM frame transmissions, in Figs. 13, 14 and 15 we provide the performance results for the receiver with four elements. For the target average BER set to $10^{-2} - 10^{-3}$, we note that a good performance is achieved for all three transmissions (a, b, and c in Figs. 13, 14 and 15, respectively), since Scheme 2 successfully tracks the underlying channel variations. Due to large propagation delays and channel variations (the coherence time on the order of seconds) that impose severe limitations on channel prediction, the adaptive scheme tends to oscillate in performance around the target BER. In Figs. 16, 17 and 18, we illustrate the channel frequency response, the allocated power and modulation levels across the data sub-carriers, respectively. A high attenuation in the frequency region $30 - 35$ kHz is mainly due to the cutoff frequency of the hydrophones which is located around 30 kHz, resulting in a severe roll-off across the upper part of the operational bandwidth. We emphasize that this system limitation was not known *a priori*, and the whole operational bandwidth ($25 - 35$ kHz) was used for OFDM transmissions. However, Scheme 2 has successfully demonstrated the ability to adapt to the system limitations by allocating the power and modulation levels to the lower part of the frequency region as illustrated in Figs. 17 and 18. Note that the channel gain at the frequency of 30.55 kHz is sufficiently high to allow the algorithm to allocate a QPSK symbol. Since the transition band of the hydrophone filter is not sharp, we can note an active tone located at 35 kHz; this artifact

results from a sufficiently high channel gain present at the given frequency.

VI. Conclusions

In this paper we explored design aspects for adaptive OFDM modulation over time-varying UWA channels. First, we investigated the possibility of predicting an UWA channel at least one travel time ahead. The key step in providing a stable reference for channel prediction is compensation of the motion-induced phase offset. Matching pursuit algorithms are used to identify the significant path coefficients, which are then processed by a low-order adaptive RLS predictor to account for large prediction lags (long feedback delays). Second, assuming that the channel is predicted one travel time ahead with a given accuracy, approximate expressions for the BER of each sub-carrier (or a cluster of adjacent sub-carriers) are obtained. From these expressions, a set of thresholds is obtained that determine the modulation level and the power needed on each sub-carrier in order to maximize the throughput while keeping the average BER at the target level. Third, spectrally-efficient adaptive schemes (Scheme 1 and Scheme 2) are applied to allocate the modulation and the power across the OFDM sub-carriers. Finally, assuming a limited feedback channel, two competitive strategies were analyzed: one that feeds back the quantized power level for each sub-carrier/cluster, and another that feeds back the quantized estimate of the significant channel coefficients in the time domain. The second strategy is found to offer better performance, as it requires significantly fewer feedback bits. Numerical and experimental results that are obtained with recorded channels and real-time at-sea experiments, respectively, show that the adaptive modulation scheme provides significant throughput improvements as compared to conventional, nonadaptive modulation at the same power and target BER. This work leads us to conclude that adaptive modulation methods may be viable for reliable, high-rate UWA communications. To our knowledge, this is the first paper that presents adaptive modulation results for UWA links with real-time at-sea experiments.

ACKNOWLEDGMENT

The authors would like to thank Dr. James C. Preisig and Keenan R. Ball for their valuable comments, suggestions and outstanding technical assistance during the KAM11 experiment.

REFERENCES

[1] M. Stojanovic, "Underwater Acoustic Communications: Design Considerations on the Physical Layer," *IEEE/IFIP Fifth Annual Conference on Wireless On demand Network Systems and Services* (WONS 2008), Garmisch-Partenkirchen, Germany, January 2008.

[2] Z. Liu, Y. Xin, and G. B. Giannakis, "Space-Time-Frequency Coded OFDM over Frequency-Selective Fading Channels," *IEEE Trans. on Sig. Proc.*, vol. 50, no. 10, pp. 2465–2476, Oct. 2002.

[3] P. Schniter, "Low-Complexity Equalization of OFDM in Doubly Selective Channels," *IEEE Trans. on Sig. Proc.*, vol. 52, no. 4, pp. 1002–1011, Apr. 2004.

[4] S. Ohno, G. B. Giannakis, "Capacity Maximizing MMSE-Optimal Pilots for Wireless OFDM Over Frequency-Selective Block Rayleigh-Fading Channels," *IEEE Trans. on Inform. Theory*, vol. 50, no. 9, pp. 2138–2145, Sept. 2004.

[5] Y. Yao and G. B. Giannakis, "Rate-Maximizing Power Allocation in OFDM Based on Partial Channel Knoweledge," *IEEE Trans. on Wireless Commun.*, vol. 4, no. 3, pp. 1073–1083, May 2005.

[6] L. Rugini, P. Banelli, "BER of OFDM Systems Impaired by Carrier Frequency Offset in Multipath Fading Channels," *IEEE Transa. on Wireless Commun.*, vol. 4, no. 5, pp. 2279–2288, Sept. 2005.

[7] L. Rugini, P. Banelli, G. Leus, "Low-Complexity Banded Equalizers for OFDM Systems in Doppler Spread Channels," *EURASIP J. Adv. Sig. Proc.*, 2006.

[8] I. Barhumi, G. Leus, and M. Moonen, "Equalization for OFDM over Doubly-Selective Channels," *IEEE Trans. on Sig. Proc.*, vol. 54, no. 4, pp. 1445-1458, Apr. 2006.

[9] Z. Tang, R. C. Cannizzaro, G. Leus, and P. Banelli, "Pilot-Assisted Time-Varying Channel Estimation for OFDM Systems," *IEEE Trans. Sig. Proc.*, vol. 55, no. 5, pp. 2226-2238, May 2007.

[10] Y. Emre, V. Kandasamy, T. M. Duman, P. Hursky, and S. Roy, "Multi-Input Multi-Output OFDM for Shallow-Water UWA Communications," *in Proc. of Acoustic 2008*, Paris, France, July 2008.

[11] K. Fang, L. Rugini, and G. Leus, "Low-Complexity Block Turbo Equalization for OFDM Systems in Time-Varying Channels," *IEEE Trans. on Sig. Proc.*, vol. 56, no. 11, pp. 5555-5566, Nov. 2008.

[12] S. Ohno, K. A. D. Teo, "Viterbi-Type Inter-Carrier Interference Equalization for OFDM over Doubly Selective Channels," *IEICE Transactions* 92-A(8), pp. 1905–1912, 2009.

[13] B. Li, S. Zhou, M. Stojanovic, L. Freitag, and P. Willet, "Multicarrier Communications over Underwater Acoustic Channels with Nonuniform Doppler Shifts," *IEEE Journal of Oceanic Engineering*, vol. 33, No. 2, pp.198–209, April 2008.

[14] B. Li, J. Huang, S. Zhou, K. Ball, M. Stojanovic, L. Freitag, and P. Willett, "MIMO-OFDM for High Rate Underwater Acoustic Communications," *IEEE J. Ocean. Eng.*, vol. 34, no. 4, pp. 634–645, Oct. 2009.

[15] M. Stojanovic, "Low Complexity OFDM Detector for Underwater Acoustic Channels," *in Proc. IEEE Oceans'06 Conference*, Boston, MA, September 2006.

[16] M. Stojanovic, "OFDM for Underwater Acoustic Communications: Adaptive Synchronization and Sparse Channel Estimation," *in Proc. International Conference on Acoustics, Speech, and Signal Processing (ICASSP'08)*, April 2008.

[17] A. J. Goldsmith and S.-G. Chua, "Variable-Rate Variable-Power MQAM for Fading Channels," *IEEE Trans. Comm.*, vol. 45, no. 10, pp. 1218–1230, Oct. 1997.

[18] D. L. Goeckel, "Adaptive Coding for Time-Varying Channels Using Outdated Fading Estimates," *IEEE Trans. Comm.*, vol. 47, no. 6, pp. 844–855, June 1999.

[19] T. Keller and L. Hanzo, "Adaptive Multicarrier Modulation: a Convenient Framework for Time-Frequency Processing in Wireless Communications," *Proc. IEEE*, vol. 88, pp. 611–640, May 2000.

[20] P. Xia, S. Zhou, and G. B. Giannakis, "Adaptive MIMO-OFDM based on Partial Channel State Information," *IEEE Trans. Sig. Proc.*, vol. 52, no. 1, pp. 202–213, Jan. 2004.

[21] B. Krongold, K. Ramchandran, and D. Jones, "Computationally Efficient Optimal Power Allocation Algorithms for Multicarrier Communication Systems," *IEEE Trans. Commun.*, vol. 48, pp. 23–27, Jan. 2000.

[22] S. Mani, T. M. Duman, and P. Hursky, "Adaptive Coding/Modulation for Shallow-Water UWA Communications," *in Proc. of Acoustic 2008*, Paris, France, July 2008.

[23] A. Radosevic, T. M. Duman, J. G. Proakis, and M. Stojanovic, "Adaptive OFDM for Underwater Acoustic Channels with Limited Feedback," *"in Proc. 45th Asilomar Conference on Signals, Systems and Computers*, November 2011.

[24] A. Radosevic, T. M. Duman, J. G. Proakis, and M. Stojanovic, "Channel Prediction for Adaptive Modulation in Underwater Acoustic Communications," *in Proc. IEEE Oceans'11 Conference*, Santander, Spain, June 2011.

[25] A. Radosevic, J. G. Proakis and M. Stojanovic, Statistical Characterization and Capacity of Shallow Water Acoustic Channels, *Proc. IEEE Oceans09 Conference*, Bremen, Germany, May 2009.

[26] D. G. Manolakis, V. K. Ingle, and S. M. Kogon, *Statistical and Adaptive Signal Processing*, New York: McGraw–Hill, 2000.

[27] W. Li and J. Preisig, "Estimation of Rapidly Time-Varying Sparse Channels," *IEEE J. Ocean. Eng.*, vol. 32, no. 4, pp. 927–939, Oct. 2007.

[28] R. M. Corless, G. H. Gonnet, D. E. G. Hare, D. J. Jeffrey, and D. E. Knuth, "On the Lambert W Function," *Adv. Comput. Math. 5*, pp. 329–359, 1996.

[29] R. F. H. Fisher and J. B. Huber, "A New Loading Algorithm for Discrete Multitone Transmission," *in Proc. Globecom '96*, London, U.K., pp. 724–728, Nov. 1996.

[30] J. Campello, "Practical Bit Loading for DMT," *in Proc. Int. Conf. Communications (ICC99)*, Vancouver, BC, Canada, vol. 2, pp. 801-805, Jun 1999.

[31] S. Golomb, “Run-Length Encodings, “ *IEEE Trans. Informar. Theory*, vol. 24, pp. 399–401, May 1966.

[32] J. Ziv and A. Lempel, “A Universal Algorithm for Sequential Data Compression,” *IEEE Trans. Informar. Theory*, vol. 24, pp. 337–343, May 1977.

[33] S. Mehrotra, “On the Implementation of a Primal-Dual Interior Point Method,” *SIAM Journal on Optimization*, vol. 2, no. 4, pp. 575–601, 1992.

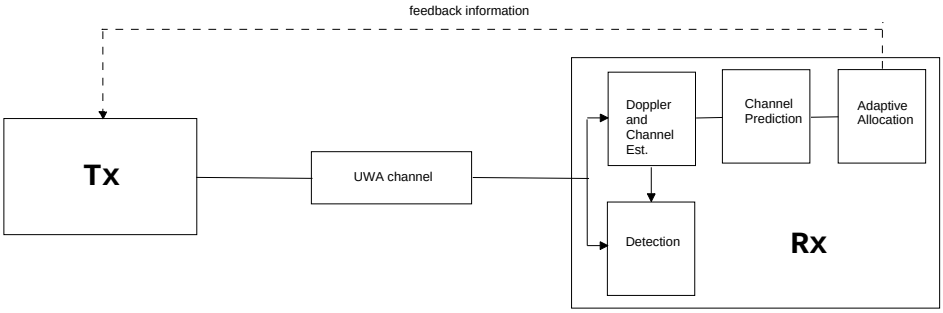

Fig. 1. The adaptive system with the important functional blocks.

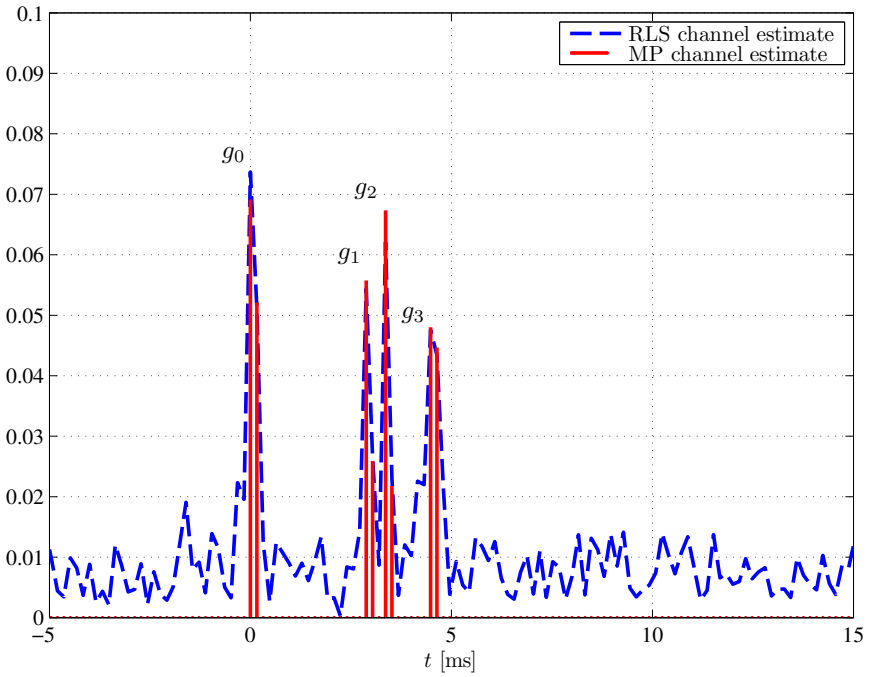

Fig. 2. Channel estimates obtained by the RLS and the MP algorithm.

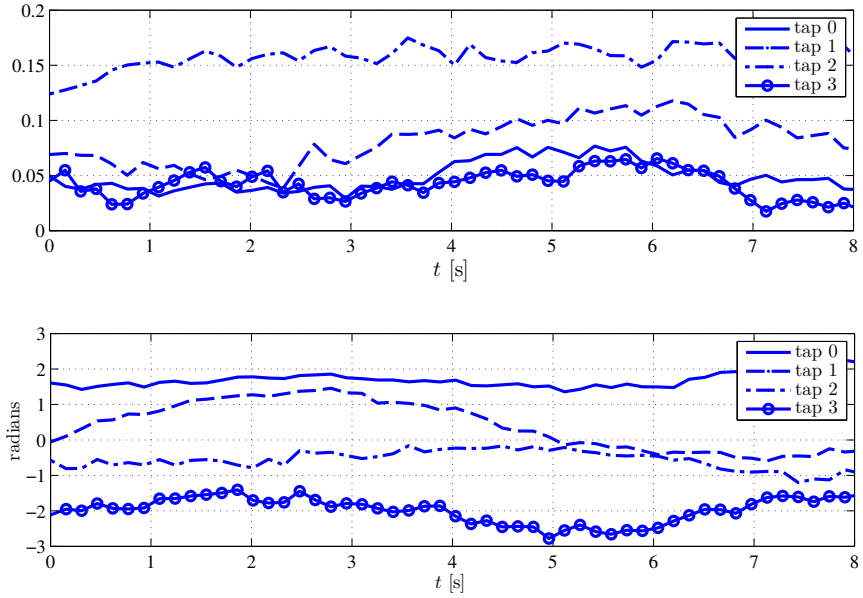

Fig. 3. Magnitudes (top) and phases (bottom) of the channel path coefficients.

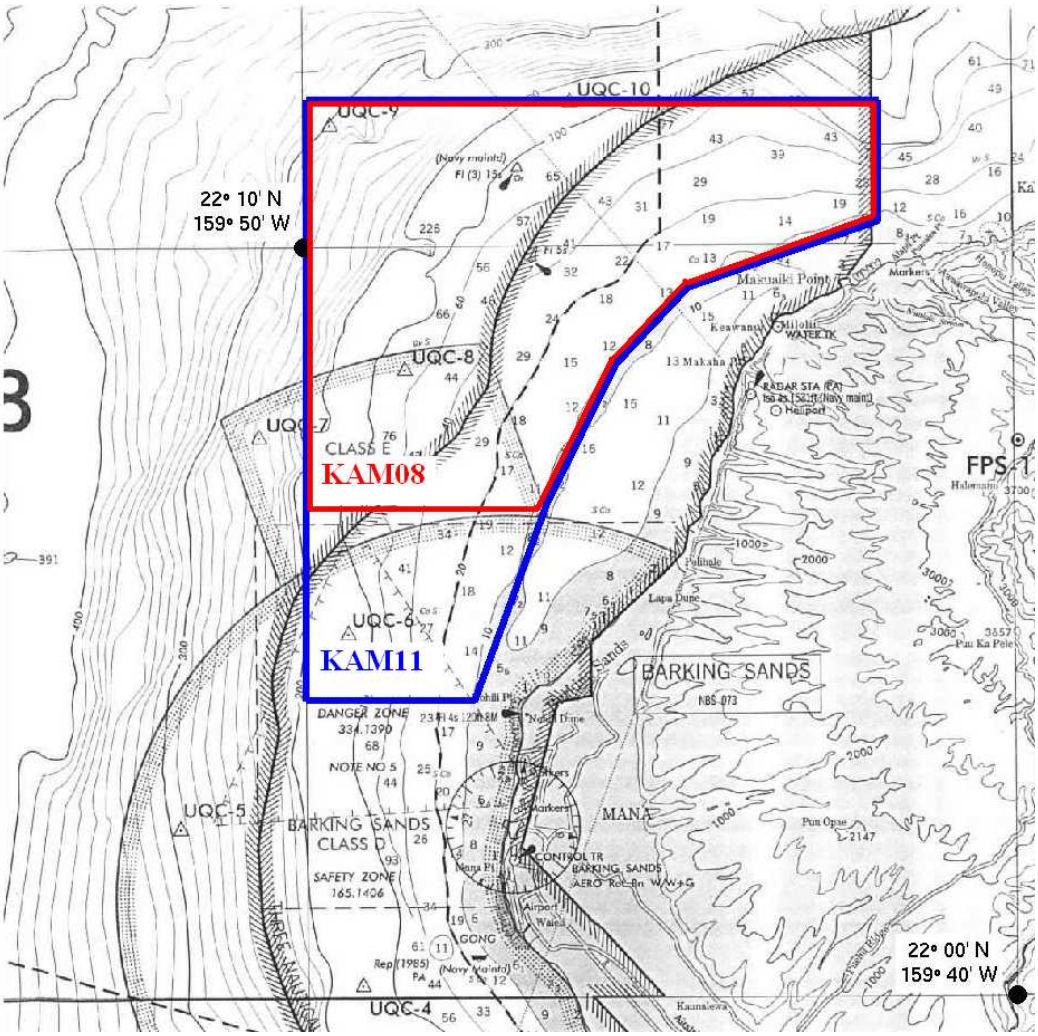

Fig. 4. The KAM08 and KAM11 operational areas are outlined by the red and blue solid lines, respectively.

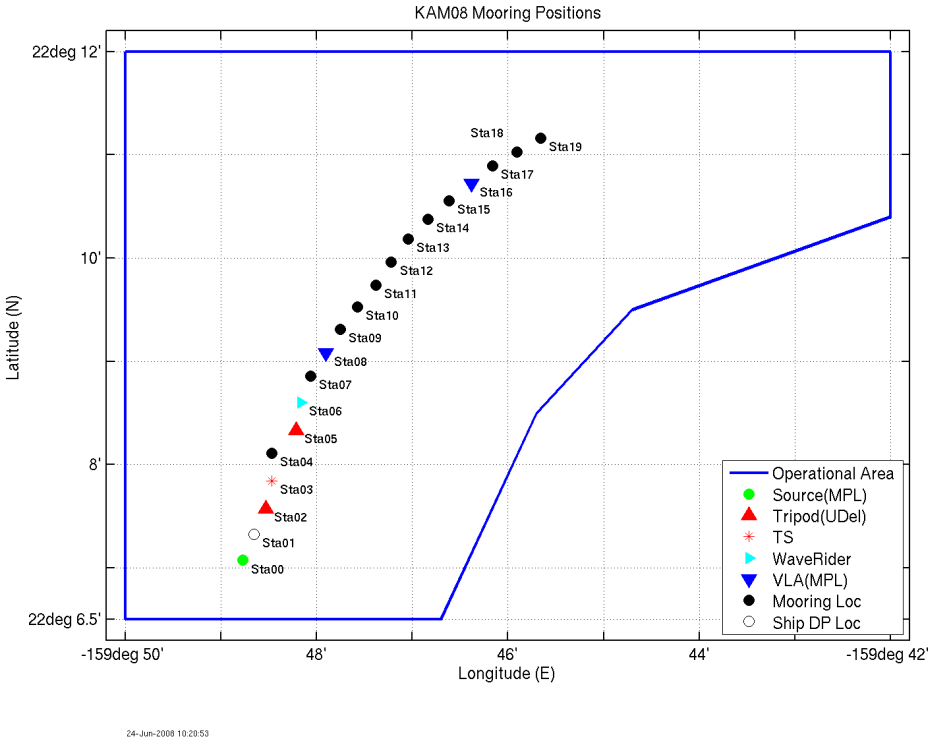

Fig. 5. Mooring deployment positions during the KAM08 in latitude and longitude. The acoustic source array was located at Sta00, while the VLAs were located at Sta08 and Sta16.

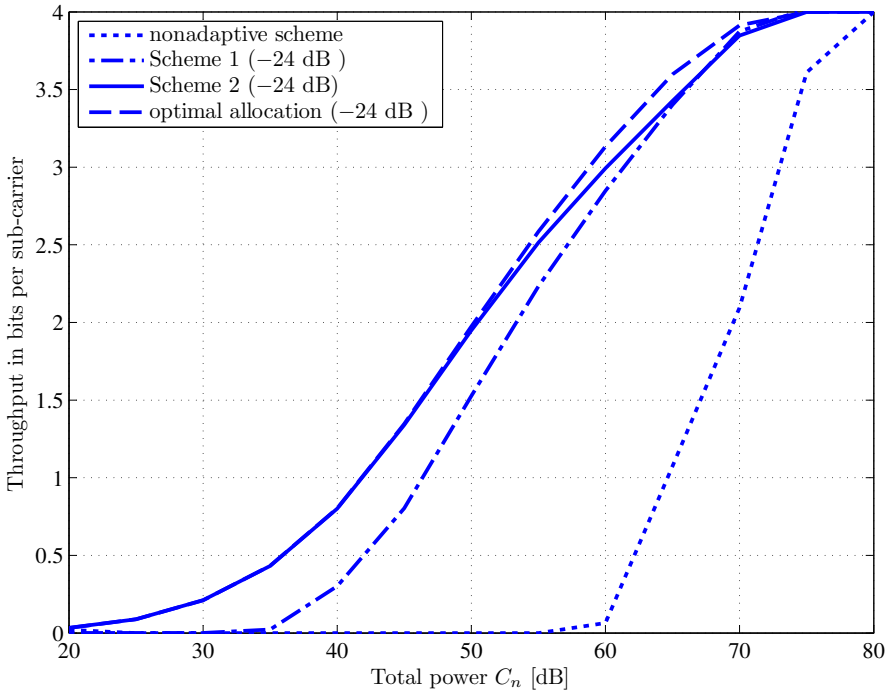

Fig. 6. Throughput performance of the various schemes considered.

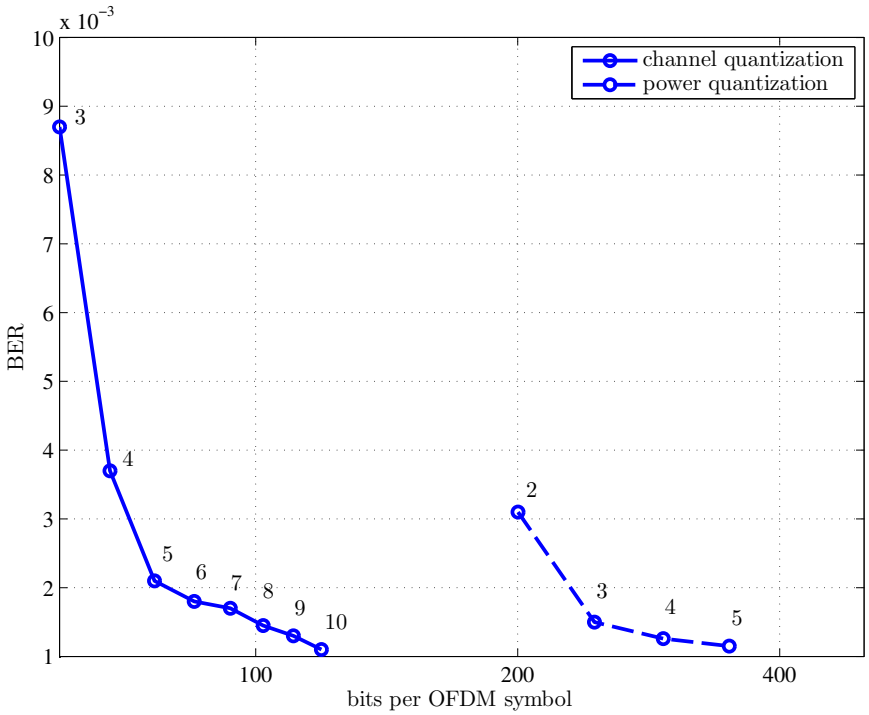

Fig. 7. Performance of limited feedback for Scheme 2 with $Q = 1$, overall power C_n of 60 dB and average throughput of 3 bits per sub-carrier. Numbers on the graph indicate the number of bits that are used to represent the quantized power levels (dashed line), and the real and the imaginary parts of each quantized channel coefficient (solid line).

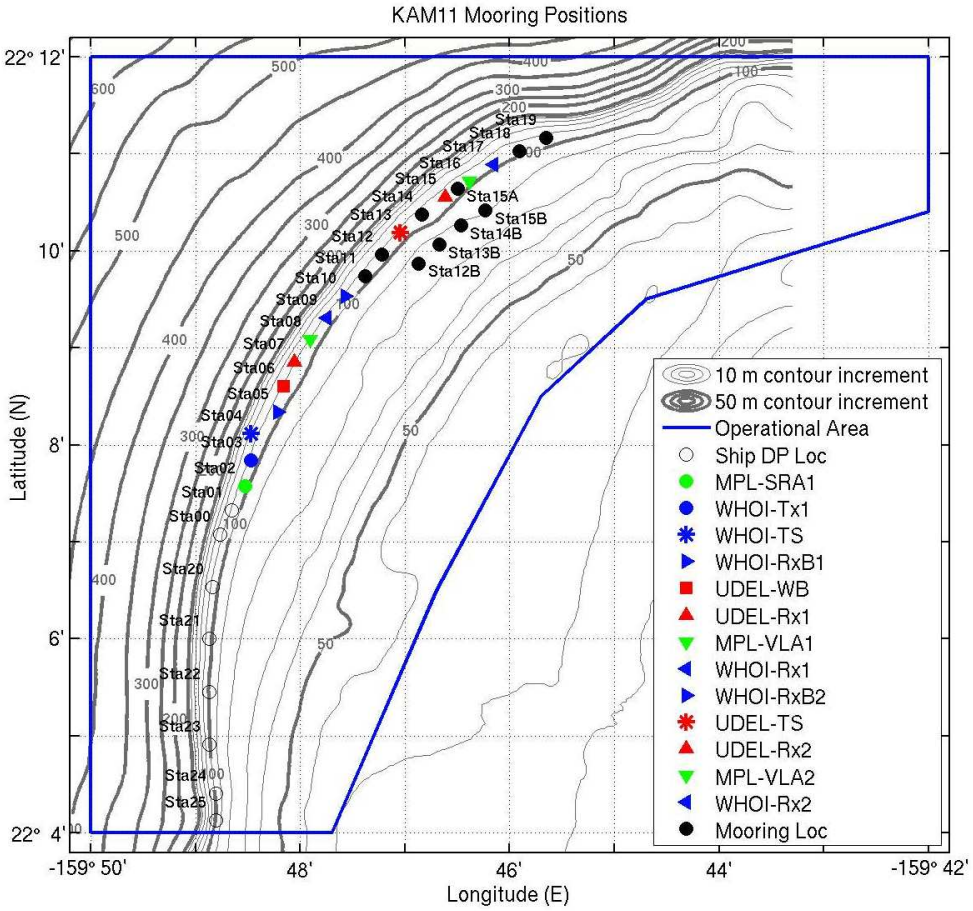

Fig. 8. Mooring deployment positions during the KAM11 in latitude and longitude. The VLAs were located at Sta05 and Sta10. The acoustic source array was located at the ship and used when the ship is stationary.

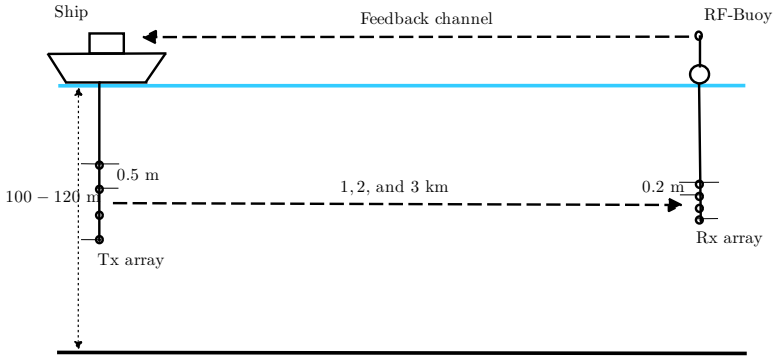

Fig. 9. The geometry and the setup of the adaptive system.

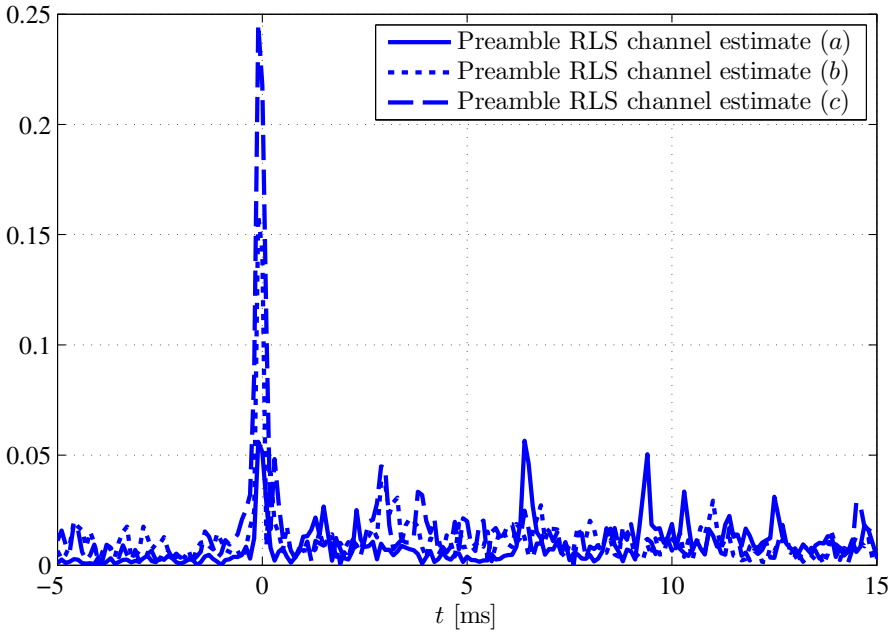

Fig. 10. Channel estimates from initial frame synchronization preamble for three consecutive non-adaptive OFDM frame transmissions. The average time interval between two consecutive frame transmissions is (roughly) 20 s.

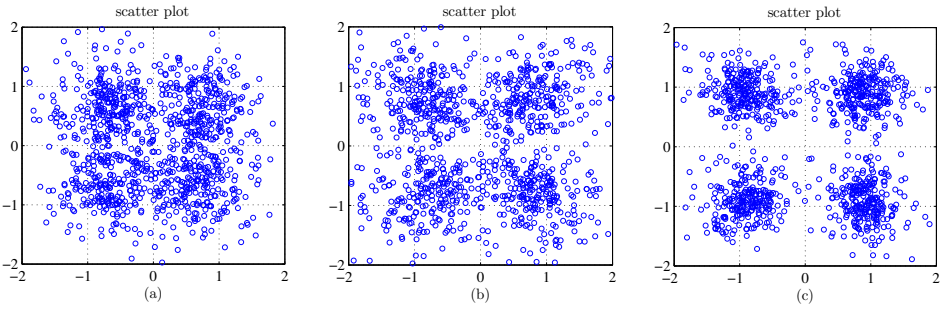

Fig. 11. Scatter plots for three consecutive non-adaptive OFDM frame transmissions, each containing 4 OFDM blocks. The average time interval between two consecutive frame transmissions is (roughly) 20 s. The corresponding channel impulse response estimates are given in Fig. 10.

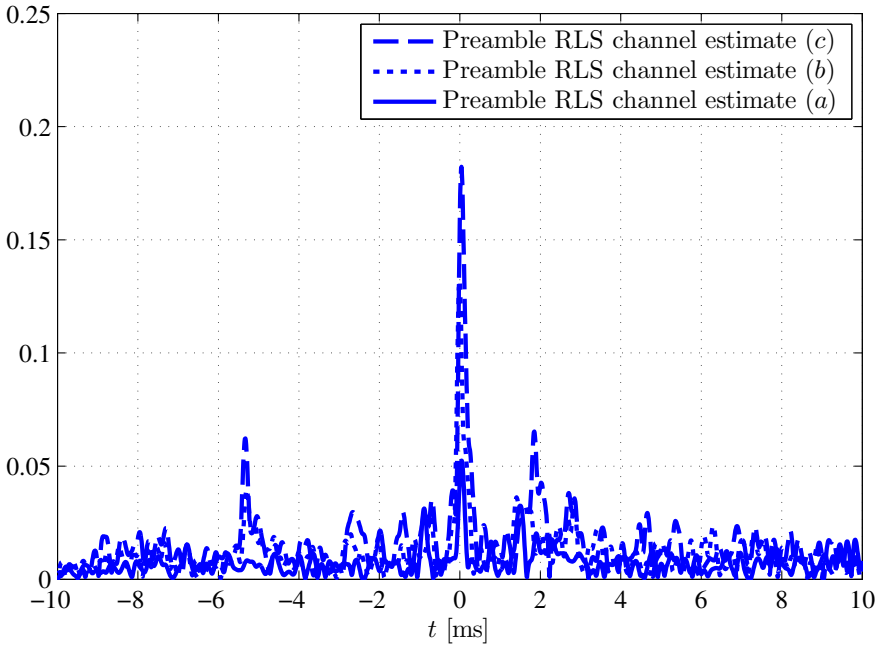

Fig. 12. Channel estimates from initial frame synchronization preamble for three consecutive adaptive OFDM frame transmissions. The average time interval between two consecutive frame transmissions is (roughly) 20 s.

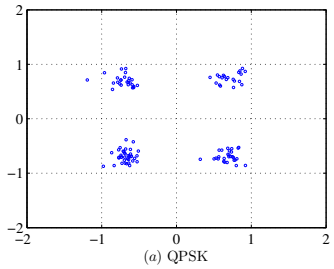

Fig. 13. Scatter plot (a) for the first adaptive OFDM frame transmission, each containing 4 OFDM blocks. The adaptive Scheme 2 allocates only QPSK modulation alphabet to the data-sub-carriers.

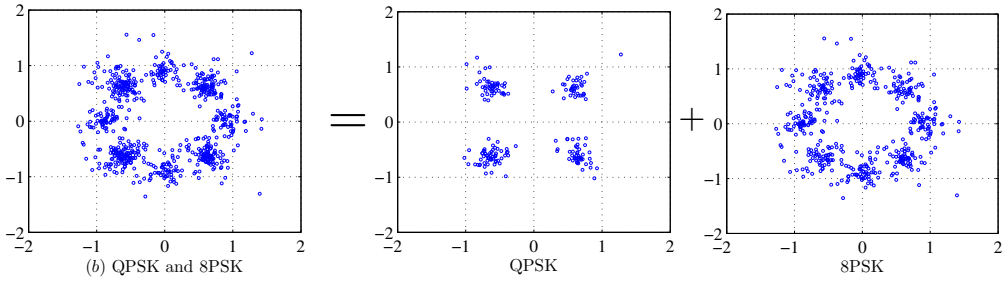

Fig. 14. Scatter plot (b) for the second adaptive OFDM frame transmission, each containing 4 OFDM blocks. The adaptive Scheme 2 allocates QPSK and 8PSK modulation alphabets to the data-sub-carriers.

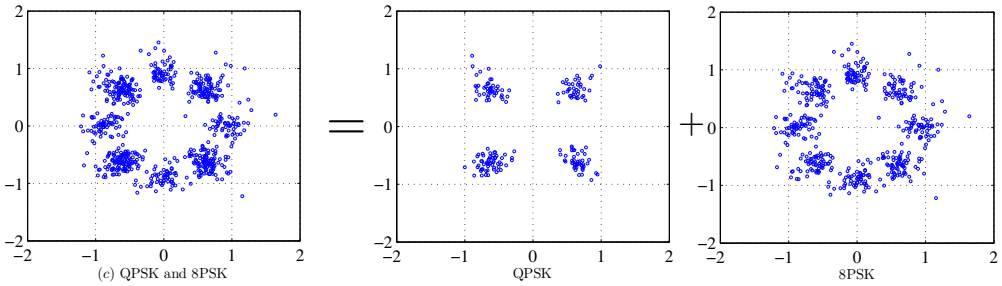

Fig. 15. Scatter plot (c) for the third adaptive OFDM frame transmission, each containing 4 OFDM blocks. The adaptive Scheme 2 allocates QPSK and 8PSK modulation alphabets to the data-sub-carriers.

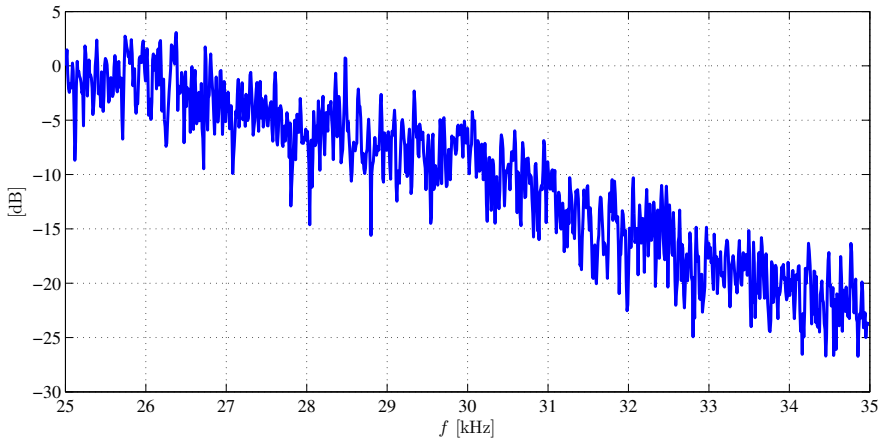

Fig. 16. A sample estimate of the channel frequency response for the OFDM system with $K = 1024$ sub-carriers.

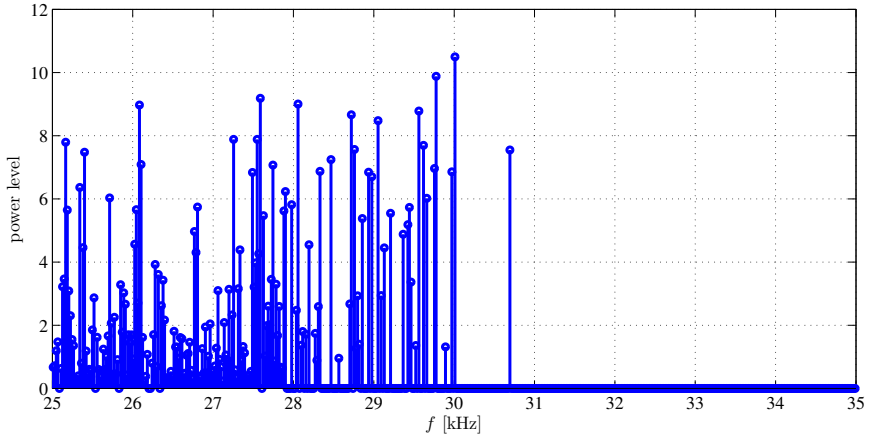

Fig. 17. A sample power allocation for data sub-carriers based on Scheme 2 and the channel response from Fig. 16.

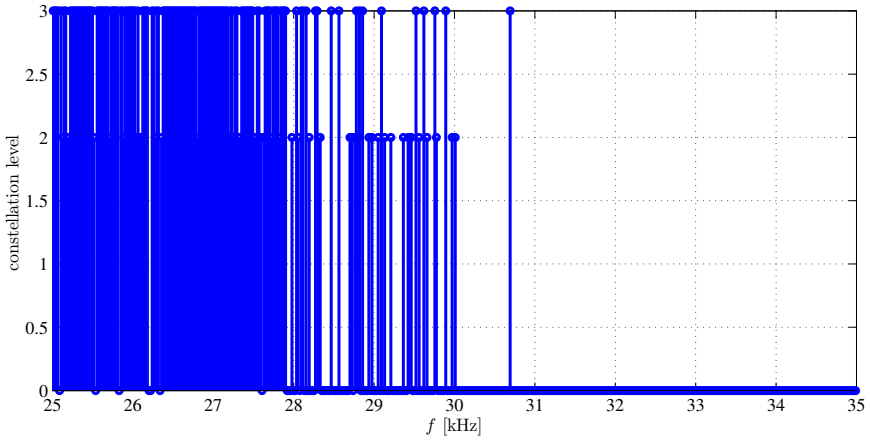

Fig. 18. A sample constellation level allocation for data sub-carriers based on Scheme 2 and the channel response from Fig. 16.

TABLE I
PREDICTION RLS ALGORITHM

The algorithm initialization:

$$\mathbf{W}[0] = \mathbf{0} \tag{20}$$

$$\mathbf{R}[0] = \delta^{-1}\mathbf{I} \ (\delta \text{ is a small positive constant}) \tag{21}$$

The joint RLS algorithm (for $n = 1, 2, \ldots$):

$$\mathbf{k}[n] = \frac{\lambda^{-1}\mathbf{R}[n-1]\tilde{\mathbf{g}}_M[n-1]}{1+\lambda^{-1}\tilde{\mathbf{g}}_M^H[n-1]\mathbf{R}[n-1]\tilde{\mathbf{g}}_M[n-1]} \tag{22}$$

$$\hat{\mathbf{g}}[n] = \mathbf{W}[n-1]\tilde{\mathbf{g}}_M[n-1] \tag{23}$$

$$\mathbf{e}[n] = \tilde{\mathbf{g}}[n] - \hat{\mathbf{g}}[n] \tag{24}$$

$$\mathbf{W}[n] = \mathbf{W}[n-1] + \mathbf{k}^H[n]\mathbf{e}[n] \tag{25}$$

$$\mathbf{R}[n] = \lambda^{-1}(1 - \mathbf{k}[n]\tilde{\mathbf{g}}_M^H[n-1])\mathbf{R}[n-1] \tag{26}$$

TABLE II
MODULATION LEVEL ALLOCATION

Initialization (for $k = 0, \ldots, K-1$**):**

$$C_{k,0} = \frac{C_n}{K};\ \mathcal{M}_{k,0} = 1; \tag{27}$$

Iterative algorithm (for $n = 1, 2, \ldots$**):**

Step 1 (for $k = 0, \ldots, K-1$**):**

$$\mathcal{M}_{k,n} = \mathcal{M}_{k,n-1}; C_{k,n} = \frac{C_n}{K}; \tag{28}$$

$$P_e = \frac{1}{K}\sum_{k=0}^{K-1} P_{e,k}(\mathcal{M}_{k,n}); \tag{29}$$

$$s_0 = \text{sign}(P_b - P_e); s = s_0; s_1 = 0; \tag{30}$$

Step 2 (for $k = 0, \ldots, K-1$**):**

if $(s = -1\ \&\ \mathcal{M}_{k,n} = 1) \quad \Delta P_{e,k} = 1;$ (31)

elseif $(s = 1\ \&\ \mathcal{M}_{k,n} = 16) \quad \Delta P_{e,k} = 1;$ (32)

else $\Delta P_{e,k} = P_{e,k}(2^s \mathcal{M}_{k,n}) - P_{e,k}(\mathcal{M}_{k,n});$ (33)

Step 3:

$$k_s^* = \min_k \arg\left\{\Delta P_{e,k}\right\}; \tag{34}$$

if $(s_1 = 1\ \&\ \Delta P_{e,k_s^*} = 1)$ **end**; (35)

elseif $(\Delta P_{e,k_s^*} = 1)$ **go to Step 4**; (36)

$$P_e = P_e + \frac{1}{K}\Delta P_{e,k_s^*};\ \mathcal{M}_{k_s^*,n} = 2^s \mathcal{M}_{k_s^*,n}; \tag{37}$$

if $(s_1 = 0)\ \ s = -s;$ (38)

if $(s_1 = 0\ \&\ s \neq s_0)$ **go to Step 2**; (39)

if $(s_1 = 0\ \&\ k_s^* \neq k_{-s}^*)$ **go to Step 2**; (40)

Step 4:

if $(s_1 = 0)$ (41)

$s_0 = \text{sign}(P_b - P_e); s = s_0; s_1 = 1;$

if $(\text{sign}(P_e - P_b) = s_0)$ **end**; (42)

go to Step 2; (43)

TABLE III
MODULATION AND POWER LEVEL ALLOCATION

Initialization (for $k = 0, \ldots, K-1$**):**

$$C_{k,0} = 0; \mathcal{M}_{k,0} = 1; \tag{44}$$

Iterative algorithm (for $n = 1, 2, \ldots$**):**

Step 1 (for $k = 0, \ldots, K-1$**):**

$$\mathcal{M}_{k,n} = \mathcal{M}_{k,n-1}; C_{k,n} = C^*_{k,n}(\mathcal{M}_{k,n}); \tag{45}$$

$$C_{all,n} = \sum_k C_{k,n}; \tag{46}$$

$$s_0 = \text{sign}(C_n - C_{all,n}); s = s_0; s_1 = 0; \tag{47}$$

Step 2 (for $k = 0, \ldots, K-1$**):**

if $(s = -1 \ \& \ \mathcal{M}_{k,n} = 1) \quad \Delta C_k = \infty;$ (48)

elseif $(s = 1 \ \& \ \mathcal{M}_{k,n} = 16) \quad \Delta C_k = \infty;$ (49)

else $\Delta C_k = C^*_{k,n}(2^s \mathcal{M}_{k,n}) - C_{k,n};$ (50)

Step 3:

$$k^*_s = \min_k \arg \{\Delta G_k\}; \tag{51}$$

if $(s_1 = 1 \ \& \ \Delta C_{k^*_s} = \infty)$ **end**; (52)

elseif $(\Delta C_{k^*_s} = \infty)$ **go to Step 4**; (53)

$$C_{all,n} = C_{all,n} + \Delta C_{k^*_s}; \tag{54}$$

$$C_{k^*_s,n} = C_{k^*_s,n} + \Delta C_{k^*_s}; \mathcal{M}_{k^*_s,n} = 2^s \mathcal{M}_{k^*_s,n}; \tag{55}$$

if $(s_1 = 0) \quad s = -s;$ (56)

if $(s_1 = 0 \ \& \ s \neq s_0)$ **go to Step 2**; (57)

if $(s_1 = 0 \ \& \ k^*_s \neq k^*_{-s})$ **go to Step 2**; (58)

Step 4:

if $(s_1 = 0)$ (59)

$$s_0 = \text{sign}(C_n - C_{all,n}); s = s_0; s_1 = 1;$$

if $(\text{sign}(C_{all,n} - C_n) = s_0)$ **end**; (60)

go to Step 2; (61)